

Two-Dimensional hybrid perovskites sustaining strong polariton interactions at room temperature

A. Fieramosca^{1,2a}, L. Polimeno^{1,2,4a}, V. Ardizzone^{1,2b}, L. De Marco^{1,c}, M. Pugliese¹, V. Maiorano¹, M. De Giorgi¹, L. Dominici¹, G. Gigli^{1,2}, D. Gerace^{3,1}, D. Ballarini¹, D. Sanvitto^{1,4}.

¹*CNR Nanotec, Institute of Nanotechnology, via Monteroni, 73100 Lecce, Italy.*

²*Dipartimento di Matematica e Fisica, Università del Salento, via Arnesano, 73100 Lecce, Italy.*

³*Dipartimento di Fisica, Università degli Studi di Pavia, via Bassi 6, 27100 Pavia, Italy. and*

⁴*INFN Istituto Nazionale di Fisica Nucleare, Sezione di Lecce, 73100 Lecce, Italy.*

Abstract

Polaritonic devices exploit the coherent coupling between excitonic and photonic degrees of freedom to perform highly nonlinear operations with low input powers. Most of the current results exploit excitons in epitaxially grown quantum wells and require low temperature operation, while viable alternatives have yet to be found at room temperature. Here we show that large single-crystal flakes of two-dimensional layered perovskite are able to sustain strong polariton nonlinearities at room temperature with no need to be embedded in an optical cavity. In particular, exciton-exciton interaction energies are measured to be remarkably similar to the ones known for inorganic quantum wells at cryogenic temperatures, and more than one order of magnitude larger than alternative room temperature polariton devices reported so far. Thanks to their easy fabrication, large dipolar oscillator strengths and strong nonlinearities, these materials hold great promises to realize actual polariton devices at room temperature.

^a These authors equally contributed to this work

^b Electronic Address: v.ardizzone85@gmail.com

^c Electronic Address: luisa.demarco@nanotec.cnr.it

I. INTRODUCTION

In efficient communication and computing systems, information carriers are required to both travel long distances without losing coherence and simultaneously interact between them in order to implement logic functions such as switches or logic gates. Microcavity polaritons, quasiparticles that form in a semiconductor when an elementary excitation field interacts sufficiently strongly with the electromagnetic radiation field, could in principle fulfill these requirements and are promising candidates for a new generation of optoelectronic devices. Indeed, these “dressed” photons exhibit enhanced non-linearities thanks to their electronic component [1, 2], allowing many-body effects to be studied in optical systems and appearing as building blocks for integrated photonic circuits and electro-optic applications [3, 4]. However, to bring strong nonlinearities and good optical properties to room temperature is a real challenge. Recently, polariton condensation and superfluidity have been observed at room temperature (RT) in organic semiconductors thanks to the very large binding energy and oscillator strength of Frenkel excitons [5]. However, interactions among excitons in organic materials are usually at least two orders of magnitude lower than the ones observed for typical Wannier-Mott excitons, and the spin degree of freedom, that is of paramount importance for photonic applications, is quickly averaged out. On the other hand, polaritons in layered transition metal dichalcogenide (TMD) materials have been anticipated to be a possible way-out, as recently demonstrated [6], showing interactions at least ten times higher than organic materials. However, they require to work with single monolayers, difficult to control and hardly reaching extensions of more than several tens of μm .

From a wider perspective, hybrid organic-inorganic perovskite systems have recently attracted a considerable attention driven by exceptional progress in photovoltaics, photonics, and optoelectronics [7–10]. In particular, two-dimensional (2D) perovskites are spontaneous realizations of multiple layered quantum well (QW) hetero-structures made of $[PbX_6]^{2-}$ tetrahedral inorganic layers, with X indicating an halide, sandwiched between bilayers of organic cations (see figure 1a) [11, 12]. The lowest-energy electronic excitations are associated to the inorganic sheet, the organic part acting as a potential barrier [7, 8, 13, 14]. In fact, these 2D layered structures share strong similarities with multi-quantum well heterostructures made of epitaxially grown inorganic semiconductors, but they possess larger binding energies and display stronger dielectric confinement in the inorganic layers. 2D

hybrid perovskites show also enhanced collective effects due to the large number of layers stacked in a single crystal, which is an advantage over TMD monolayers. Strong light-matter coupling has already been observed in $MAPbBr_3$ micro/nanowire cavities [15]; in particular, evidence for exciton-polariton effects has been reported in all-inorganic perovskite $CsPbX_3$ nanoplatelets, nanowires [16, 17] and in spin-coated layered hybrid organic-inorganic perovskite thin films [18–20]. These results indicate a huge room for substantial advancements in the realization of low threshold coherent light sources and polaritonic devices with this kind of hybrid organic-inorganic semiconductors [21].

Here we address, for the first time, the nonlinear properties of polaritons in monocrystalline 2D hybrid perovskites by directly estimating the exciton-exciton interaction energy. The understanding and control of this property is of paramount importance to assess the material potentialities for room temperature polaritonics, such as all-optical transistors, switches and gates, up to now only demonstrated at cryogenic temperatures in GaAs based semiconductors. To this aim, we employ large flakes of high-quality 2D perovskite single crystals to directly measure the excitonic response without being limited by non-radiative losses and grain-to-grain heterogeneity, usually present in polycrystalline films. Remarkably, at room temperature we find the exciton oscillator strengths to be much larger than in epitaxial GaAs QWs at cryogenic temperatures, and with comparable nonlinearities. Most importantly, thanks to the large oscillator strength of the excitons, and the very good crystal structure of the flakes, formation of polaritonic bands and strong nonlinearities are observed even when these structures are not embedded in a microcavity. This is an important step towards the realization of polaritonic devices working at room temperature with easy fabrication and minimal processing, avoiding complex heterostructures comprising top and bottom Bragg mirrors.

II. RESULTS AND DISCUSSION

We synthesize phenethylammonium lead iodide ($C_6H_5(CH_2)_2NH_3$) $_2PbI_4$ (PEAI) by an Anti-solvent Vapor assisted Crystallization method [22] and subsequent mechanical exfoliation [11]. In this work, we study both PEA single crystals embedded in an optical cavity formed by two Distributed Bragg Reflectors (DBR) acting as bottom/top mirrors and bare single crystals. Figure 1a shows a sketch of a single 2D PEA single crystal grown on a DBR

formed by seven $\text{SiO}_2/\text{TiO}_2$ pairs. A second DBR also formed by seven $\text{SiO}_2/\text{TiO}_2$ pairs is sputtered on the single crystal in order to give rise to an optical Fabry-Perot cavity in which the PEAI 2D crystal is embedded. The optical response of the sample is measured in transmission geometry, the excitation being provided by a non-resonant continuous wave laser or a femtosecond pulsed laser resonant on the low polariton branch (see also Supplementary Information).

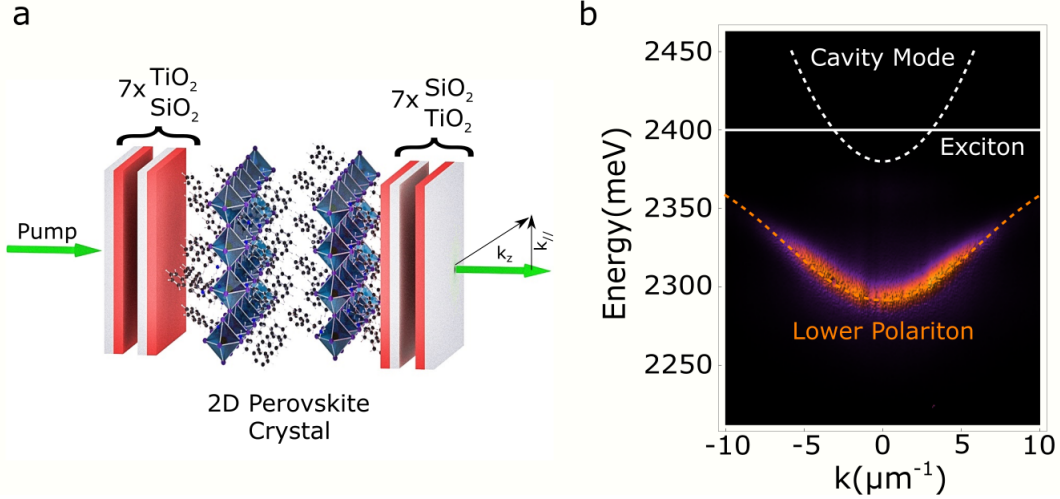


Figure 1. a) Schematic representation of a 2D perovskite single crystal embedded in an optical cavity formed by two distributed Bragg reflectors; in 2D perovskite inorganic layers are separated by organic ligands realizing an effective multiple layered quantum well structure; b) Energy versus in-plane momentum k photoluminescence emission from the sample represented in figure 1a, with $k = \frac{2\pi}{\lambda} \sin\theta$, θ being the emission angle; the white dashed and solid lines represent respectively the cavity and the exciton uncoupled modes, the orange line is a fit to the polariton lower mode with $E_X = 2.395$ eV, $E_C = 2.385$ eV and $\hbar\Omega = 170$ meV;

Figure 1b shows the energy and in-plane momentum resolved emission from this sample under non-resonant excitation. Due to the strong coupling between the cavity mode and the exciton in the PEAI single crystal, a lower polariton mode is clearly visible with an emission energy of about 2.31 eV at $k = 0$. By fitting the experimental dispersion we obtain a Rabi splitting $\hbar\Omega = 170$ meV, with an energy minimum of the cavity mode at $E_C = 2.385$ eV and an exciton energy $E_X = 2.395$ eV.

To test the polarization dependent polariton-polariton interaction in this sample, we measure the resonant transmission of a fs pulsed excitation laser through the sample at

normal incidence ($k=0$). Figure 2a shows the transmission when the laser is linearly polarized and figure 2b shows the transmission when the laser is circularly polarized. Each spectrum in figure 2a and 2b corresponds to different excitation powers, P . As the excitation power increases, we observe a shift of the transmission peak towards higher energies. The energy blueshift of the transmission peaks is plotted in figure 2c against the excitation power. As the excitation power increases, we observe a shift of the transmission peak towards higher energies as expected for a system of interacting particles [16, 23], the polariton density inside the active medium being proportional to the incident power. Moreover, figure 2c shows that the energy blueshift obtained with a circularly polarized laser (blue dots) is higher than the blueshift measured with a linearly polarized laser (red dots). In other words, the observed energy blueshift is sensitively larger when all the polaritons are created with the same spin [24–27]. Instead, by using a linear polarized laser (i.e. a coherent superposition of two counter-polarized circular components), only half of the excited polaritons share the same spin, thus roughly halving the interaction energy. We notice that the polarization properties of the elementary excitations in these materials arise from the optical transitions connecting the valence band s-type states with total angular momentum quantum numbers ($J = 1/2, J_z = \pm 1/2$) to p-type conduction band states with the same symmetry (due to the spin-orbit splitting in the conduction band) [28, 29]. Hence, bright exciton states correspond to optical transitions satisfying the condition $\Delta J_z = \pm 1$, which can be excited by using either clockwise or counter-clockwise circularly polarized radiation. As a consequence, polariton states are formed with ± 1 spin polarization, in close analogy to inorganic semiconductor exciton-polaritons in microcavities with embedded quantum wells.

The observed spin-dependence is then a strong indication that polariton-polariton interactions not only are the dominant effect responsible for the energy shift of the modes upon optical excitation but also that 2D perovskites can be used for polariton spintronics. The dashed lines in figure 2c are obtained as a linear fit to the experimental points. The ratio between the two slopes is $L/C = 0.47 \pm 0.06$. By following Vladimirova et al. [25] we can extract the ratio α_2/α_1 from the data of figure 2c, in which α_2 is the interaction strength between polaritons having opposite spin and α_1 is the interaction strength between polaritons having the same spin. We deduce then from figure 2c a ratio $|\alpha_2/\alpha_1| \sim 0.05$. This value is consistent with the picture of polariton-polariton interactions in standard semiconductors at cryogenic temperature, i.e., a strong repulsive interaction for polaritons having the same

spin ($\alpha_1 > 0$) and a weaker interaction for polaritons having opposite spin ($|\alpha_1| \gg |\alpha_2|$). Strikingly, we observe spin-dependent nonlinearities similar to those observed in GaAs based systems at cryogenic temperatures.

In the mean-field approximation and at low particle density the blueshift ΔE_{pol} depends linearly on the polariton density n_{pol} : $\Delta E_{pol} = g_{pol}n_{pol}$. The polariton density n_{pol} is proportional to the excitation power incident on the sample. By analyzing the power dependence of the blueshift it is possible to measure the polariton interaction constant and then, knowing the polariton excitonic fraction (or Hopfield coefficient) one can finally infer the excitonic interaction constant $g_{exc,lay}$ per layer. The estimated excitonic interaction constant values for the microcavity sample is $g_{exc,lay} \sim 3 \pm 0.5 \mu eV \mu m^2$ (Supplementary Information). This value is comparable with the one typically estimated for a single GaAs quantum well [30, 31] and it is the largest reported value at room temperature so far.

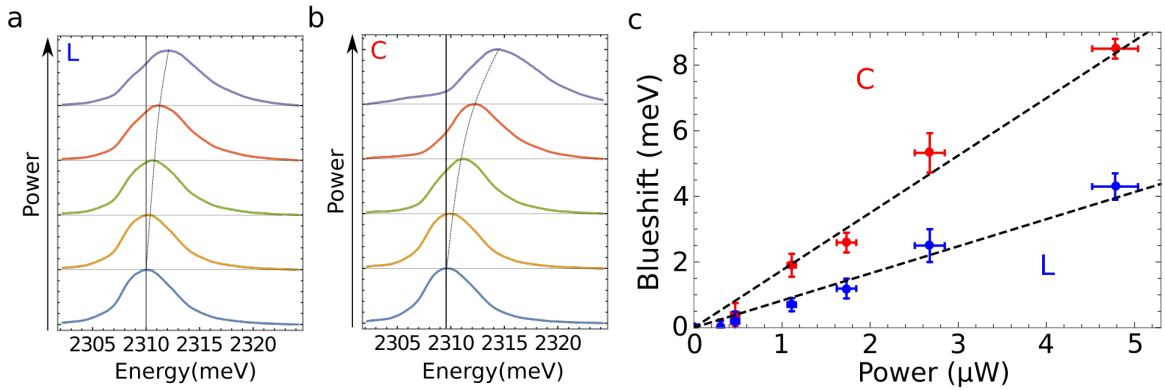


Figure 2. a) Transmittivity spectra obtained by cutting the dispersion of figure 1b in $k = 0$ and corresponding to different resonant excitation power for linear (a) and circular (b) polarized excitation laser; c) Blueshift of the polariton modes in the case of a linear (L) and a circular (C) polarized laser; the dashed lines are linear fit to the experimental data with slopes of 1.75 and 0.83 $meV/\mu W$ for C and L respectively.

The observation of polaritonic nonlinearities at RT in organic-inorganic hybrid materials is a fundamental step to assess the potential for real world polariton devices. The structure of the sample of figure 1a is complex and requires at least a three-steps fabrication process: growth of the bottom DBR mirror, growth of the single crystal flake, and finally growth of the top DBR mirror. Further developments could involve additional fabrication steps like electrical contacts for carriers injection or interconnecting several devices to provide the dif-

ferent functionalities associated with network-on-chip technology. These further steps would result in an even more complex fabrication process, possibly hindering the technological appeal of RT polaritonic devices. However, RT polaritons in 2D single crystal PEA1 flakes have been observed even if the crystal flake is not embedded in an optical cavity [28]. Single bare PEA1 crystal flakes without cavity are a relatively simpler system to grow. Moreover, the active region can be readily accessed for electrical connections, patterning or for interconnecting several devices. From a technological point of view, assessing RT polariton nonlinearities in single 2D crystals with no cavity, is of utmost importance and would lift the complication to embed the perovskite between two mirrors.

Figure 3a shows a sketch of a single 2D PEA1 crystal flake grown on a glass substrate. Figure 3b shows in-plane momentum and energy resolved reflectivity spectra obtained from the single 2D PEA1 crystal slab under white light illumination. The optical response of the sample is measured with an oil-immersion microscope objective which allows to capture, from the glass substrate side, also the signal from the total internal reflection (TIR) at the air-crystal interface (see Supplementary Information for details). Remarkably, the measured reflectivity shows a manifold of lower polariton modes (visible as dips in the reflectivity) arising from the coupling of the bare excitonic resonance (white line) with the optical resonances of the 2D slab itself [28]. The red dashed lines of figure 3b are fits to the lower polariton modes giving a value of energy coupling between the optical modes and the excitonic transition of $\hbar\Omega \sim 170$ meV. This value is larger than the linewidths of the different resonances involved and it is then fully consistent with the strong exciton-photon coupling regime [28]. In particular, strong coupling between the exciton mode and the optical resonances of the slab is obtained at room temperature thanks to the optical confinement given by the refractive index contrast at the interface between the crystal and the surrounding media (respectively air and glass substrate) and the high value of the excitonic oscillator strength in 2D perovskites.

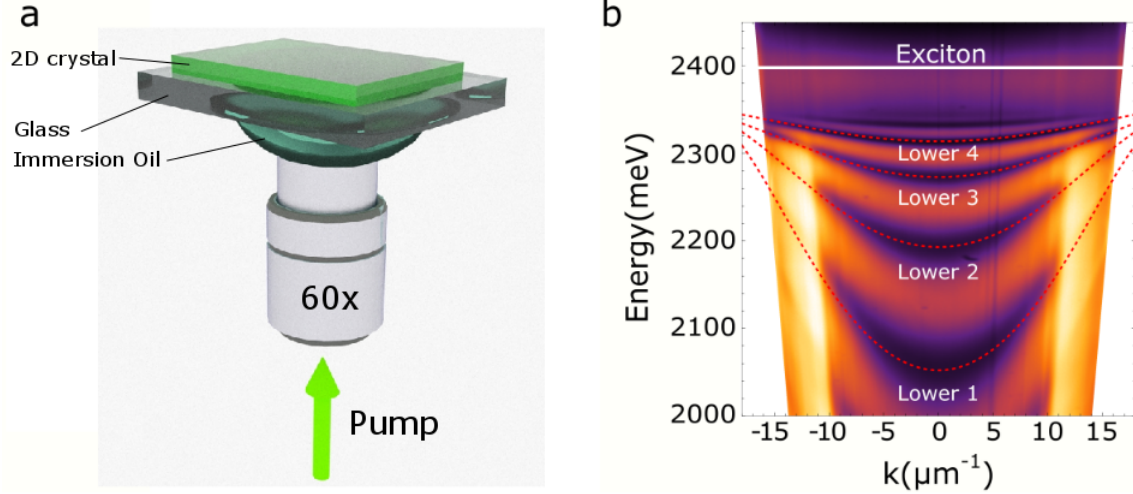


Figure 3. a) A schematic representation of the TIR configuration adopted for resonant blueshift measurements: an immersion oil objective (60x) is used to focus the excitation beam on a 2D PEAI single crystal flake grown on a glass substrate; the same objective is used to collect the reflected light; b) Energy and in-plane momentum k resolved reflectivity spectra of a thick single crystal slab of PEAI; the dips in reflectivity correspond to lower polariton modes resulting from the coupling of the exciton mode to different optical modes; the white line represents the energy of the bare exciton mode; the red dashed lines represent lower polariton modes; the enhanced intensity for $k \geq 10 \mu m^{-1}$ corresponds to angles of incidence beyond the light line between air and the perovskite slab.

In order to understand if the observed polariton modes of the bare 2D PEAI crystal can sustain nonlinearities at RT, we resonantly excite the single crystal slab with a pulsed fs laser. The excitation beam forms a finite angle with the surface of the slab, corresponding to an in-plane momentum of about $k \sim 12.7 \mu m^{-1}$. This value of in-plane momentum corresponds to an angle that is beyond the crystal-air TIR angle, which means that all the incident laser power is absorbed or reflected by the sample, the transmitted part being negligible. The green oval region in figure 4a shows the energy and momentum spread of the laser used in resonant excitation. Figure 4b represents a vertical cut of the dispersion of figure 4a corresponding to the green region.

This choice of the incident angle, in addition to being in the highest reflectivity region, allows also to probe polariton modes having a higher excitonic fraction and smaller linewidth.

The bandwidth of the fs laser is large enough to resonantly excite essentially three adjacent lower polariton branches. Figure 4b shows that the reflectivity spectra change when the incident power is increased: the low-power resonances (red continuous lines) are shifted at high incident power (blue continuous lines) and then recover their initial energy (red dashed lines) when the incident power is lowered—which guarantees that the blueshift is not due to degradation of the material upon optical excitation. This evidence shows that the observed blueshift arises from interparticle interactions, as observed in low-temperature inorganic polariton systems [24–26] and in the cavity-embedded single crystal of figure 2.

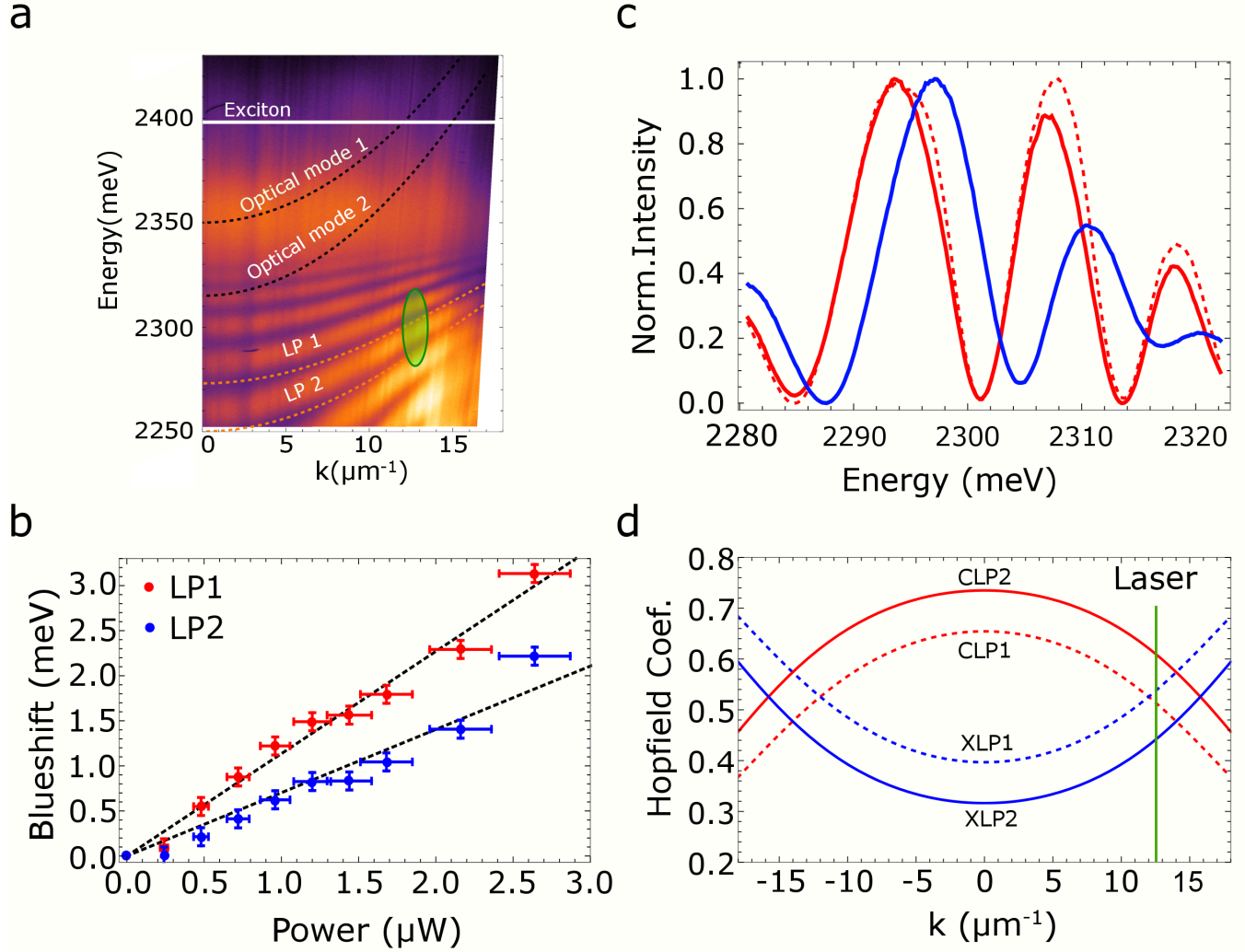


Figure 4. a) Reflectivity spectra obtained for a PEA single crystal slab; the same excitonic mode is coupled to several optical modes of the slab; the two lower polariton modes highlighted by orange dashed lines originate from the coupling of the two optical modes (black dashed lines) to the excitonic mode (white solid line); b) energy shift of the lower polariton modes of (a) as a function of the incident power and; the energy shift is measured at $k \sim 12.7 \mu\text{m}^{-1}$ corresponding to the green region of panel (a); c) reversibility of the observed blueshift of the polariton modes; the red continuous curve correspond to the energy of the polariton modes for low excitation power $P = 10 \mu\text{J}/\text{cm}^2$; the continuous blue curve shows the blueshifted modes at high excitation power $P = 150 \mu\text{J}/\text{cm}^2$; when the excitation power is reduced, the polariton modes recover the original energy (dashed red curve). d) Hopfield coefficients showing the exciton (XLP1, XLP2) and photon (CLP1, CLP2) fraction of the two lower polariton modes of (a); the green vertical line represents the in-plane momentum of the resonantly created polariton, with LP1 having a larger exciton fraction than LP2.

The TIR geometry chosen to perform resonant excitation allows us to neglect the transmission through the sample, simplifying the estimation of the incident power (see also the Supplementary Information). The two lower polariton branches fitted by the dashed orange lines (LP1 and LP2) originate from the two optical modes highlighted by the two black dashed lines. Polariton modes originating from different cavity modes and coupled to the same excitonic transition possess a different excitonic fraction at a given excitation angle. Figure 4c shows the blueshift measured for the lower polariton branches LP1 and LP2 of figure 4a as a function of the polariton density by using a linearly polarized pulsed laser. We observe that, for a given incident power (i.e. a given polariton density), the measured blueshift is higher for the polariton branch having the higher excitonic fraction, LP1, which confirms that the energy blueshift increases as the excitonic component increases. By fitting the data of figure 4c with a straight line and considering the relation between ΔE_{pol} and n_{pol} we can obtain the excitonic interaction constant per layer $g_{exc,lay}$. In fact, given the incident power values and considering that all the absorbed light is transformed into polaritons (which is a very conservative approximation, see Supporting Information) the upper density limit for the exciton density per layer is of about $n_{exc,layer} = 10^{12} \text{ cm}^{-2}$. Accounting for the different excitonic fraction of the two lower polariton branches, we obtain a value of the excitonic interaction constant $g_{exc,lay} \sim 1 \pm 0.2 \text{ } \mu\text{eV}\mu\text{m}^2$ per inorganic layer. This value is comparable with that obtained for the 2D single crystal embedded in a microcavity, as shown in Figs. 1 and 2. In both cases, we used a pulsed resonant laser to estimate the interaction constants, thus avoiding the effects of the polariton-reservoir interactions which would contribute to the blueshift observed and would forbid a direct probe of the polariton-polariton interaction constants. Moreover, we would like to stress that by neglecting any loss in the material, we overestimate the number of excitons in the system, therefore much larger interaction strengths should be expected and the reported value of g_{exc} should be taken as a lower bound. Nevertheless, this lower bound is already at least two orders of magnitude higher than typical interaction constants of organic excitons at room temperature [32] and about twenty times larger than the values recently measured in a WS_2 monolayer [6].

In summary, we have observed highly interacting polaritons in hybrid organic-inorganic 2D perovskites single crystals at room-temperature. These materials spontaneously crystallize in a multiple layered quantum well-like structure and, thanks to the high oscillator strength of the excitonic transition, strong coupling is achieved at room temperature even

without highly reflecting mirrors. The resulting polaritons are highly interacting with an excitonic interaction constant $g_{exc,lay} \geq 1 \pm 0.2 \mu eV \mu m^2$. This value is two orders of magnitudes higher than the values measured for organic excitons and it is the highest measured at room temperature so far. Moreover, we observe that polariton-polariton interactions in our sample are spin-dependent, with repulsive interaction between polaritons having the same spin being the dominant effect. These results demonstrate that 2D hybrid organic-inorganic perovskites sustain highly interacting polaritons working with interaction constants which are very promising for future polaritonic and spintronic devices at room temperature. Most important, we observe highly interacting polaritons at RT without embedding the active medium in an optical cavity. These findings are extremely important and promise to greatly reduce the cost and the complexity of fabrication and post-processing of polaritonic devices.

III. METHODS

Synthesis of 2D perovskite flakes. PEAI solutions were prepared dissolving in gammabutyrolactone equimolar amount of PbI₂ and phenethylammonium iodide, and stirring at 70°C for 1 hour. 2D perovskite single crystals were synthesized by Anti-solvent Vapor assisted Crystallization method as follows: 5 microliters of the perovskite solution are deposited on glass substrate and immediately after capped by a second glass. Then, a small vial containing 2 mL of dichloromethane is placed on the top of the two sandwiched substrates. Substrates and vial are placed in a bigger Teflon vial, closed with a screw cap and left undisturbed for some hours. After this time millimetre-sized crystals appear in between the two substrates having a thickness varying from few to ten micrometres. Single crystals are mechanically exfoliated with SPV 224PR-M Nitto Tape and transferred onto glass substrates. The exfoliated flakes, having the thickness of tens of nanometres, appear smooth and uniform over tens of square micrometers, as observed by scanning electron microscopy (SEM) and atomic force microscopy (AFM).

ACKNOWLEDGMENTS

The authors acknowledge the ERC project ElecOpteR grant number 780757 and the project “TECNOMED - Tecnopolo di Nanotecnologia e Fotonica per la Medicina di Pre-

cisione”, (Ministry of University and Scientific Research (MIUR)Decreto Direttoriale n. 3449 del 4/12/2017, CUP B83B17000010001). G.G. gratefully acknowledges the project PERSEO-PERrovskite-based Solar cells: towards high Efficiency and lOng-term stability (Bando PRIN 2015-Italian Ministry of University and Scientific Research (MIUR) Decreto Direttoriale 4 novembre 2015 n. 2488, project number 20155LECAJ). The authors acknowledge Paolo Cazzato for technical support.

- [1] P. G. Savvidis, J. J. Baumberg, R. M. Stevenson, M. S. Skolnick, D. M. Whittaker, and J. S. Roberts. Angle-resonant stimulated polariton amplifier. *Phys. Rev. Lett.*, 84:1547–1550, Feb 2000.
- [2] C. Weisbuch, M. Nishioka, A. Ishikawa, and Y. Arakawa. Observation of the coupled exciton-photon mode splitting in a semiconductor quantum microcavity. *Phys. Rev. Lett.*, 69:3314–3317, Dec 1992.
- [3] I. Carusotto and C. Ciuti. Quantum fluids of light. *Rev. Mod. Phys.*, 85:299–366, Feb 2013.
- [4] D. Sanvitto and S. Kéna-Cohen. The road towards polaritonic devices. *Nature Materials*, 15(10):1061–1073, Jul 2016.
- [5] G. Lerario, A. Fieramosca, F. Barachati, D. Ballarini, K. S. Daskalakis, L. Dominici, M. De Giorgi, S. A. Maier, G. Gigli, S. Kéna-Cohen, and D. Sanvitto. Room-temperature superfluidity in a polariton condensate. *Nature Physics*, 13(9):837–841, Jun 2017.
- [6] F. Barachati, A. Fieramosca, S. Hafezian, J. Gu, B. Chakraborty, D. Ballarini, L. Martinu, V. Menon, D. Sanvitto, and S. Kéna-Cohen. Interacting polariton fluids in a monolayer of tungsten disulfide. *Nature Nanotechnology*, 13(5):906–909, May 2018.
- [7] L. Pedesseau, D. Saponi, B. Traore, R. Robles, H.-H. Fang, M. A. Loi, H. Tsai, W. Nie, J.-C. Blancon, A. Neukirch, S. Tretiak, A. D. Mohite, C. Katan, J. Even, and M. Kepenekian. Advances and promises of layered halide hybrid perovskite semiconductors. *ACS Nano*, 10(11):9776–9786, Oct 2016.
- [8] B. Saperov and D. B. Mitzi. Organic–inorganic perovskites: Structural versatility for functional materials design. *Chemical Reviews*, 116(7):4558–4596, Apr 2016.
- [9] B. R. Sutherland and E. H. Sargent. Perovskite photonic sources. *Nature Photonics*, 10(5):295–302, May 2016.

- [10] Felix Thouin, Stefanie Neutzner, Daniele Cortecchia, Vlad Alexandru Dragomir, Cesare Soci, Teddy Salim, Yeng Ming Lam, Richard Leonelli, Annamaria Petrozza, Ajay Ram Srimath Kandada, and Carlos Silva. Stable biexcitons in two-dimensional metal-halide perovskites with strong dynamic lattice disorder. *Physical Review Materials*, 2(3), mar 2018.
- [11] W. Niu, A. Eiden, G. V. Prakash, and J. J. Baumberg. Exfoliation of self-assembled 2d organic-inorganic perovskite semiconductors. *Applied Physics Letters*, 104(17):171111, Apr 2014.
- [12] O. Yaffe, A. Chernikov, Z. M. Norman, Y. Zhong, A. Velauthapillai, A. van der Zande, J. S. Owen, and T. F. Heinz. Excitons in ultrathin organic-inorganic perovskite crystals. *Physical Review B*, 92(4), Jul 2015.
- [13] T. Ishihara, J. Takahashi, and T. Goto. Optical properties due to electronic transitions in two-dimensional semiconductors $(C_nH_{2n+1}NH_3)_2PbI_4$. *Physical Review B*, 42:11099–11107, Dec 1990.
- [14] T. Kondo, S. Iwamoto, S. Hayase, K. Tanaka, J. Ishi, M. Mizuno, K. Ema, and R. Ito. Resonant third-order optical nonlinearity in the layered perovskite-type material $(C_6H_{13}NH_3)_2PbI_4$. *Solid State Communications*, 105(8):503–506, Feb 1998.
- [15] S. Zhang, Q. Shang, W. Du, J. Shi, Z. Wu, Y. Mi, J. Chen, F. Liu, Y. Li, M. Liu, Q. Zhang, and X. Liu. Strong exciton-photon coupling in hybrid inorganic-organic perovskite micro/nanowires. *Advanced Optical Materials*, 6(2):1701032, Dec 2017.
- [16] R. Su, C. Diederichs, J. Wang, T. C. H. Liew, J. Zhao, S. Liu, W. Xu, Z. Chen, and Q. Xiong. Room-temperature polariton lasing in all-inorganic perovskite nanoplatelets. *Nano Letters*, 17(6):3982–3988, May 2017.
- [17] K. Park, J. W. Lee, J. D. Kim, N. S. Han, D. M. Jang, S. Jeong, J. Park, and J. K. Song. Light matter interactions in cesium lead halide perovskite nanowire lasers. *The Journal of Physical Chemistry Letters*, 7(18):3703–3710, Sep 2016.
- [18] T. Fujita, Y. Sato, T. Kuitani, and T. Ishihara. Tunable polariton absorption of distributed feedback microcavities at room temperature. *Phys. Rev. B*, 57:12428–12434, May 1998.
- [19] K. Pradeesh, J. J. Baumberg, and G. Vijaya Prakash. Strong exciton-photon coupling in inorganic-organic multiple quantum wells embedded low-q microcavity. *Opt. Express*, 17(24):22171–22178, Nov 2009.

- [20] A. Brehier, R. Parashkov, J. S. Lauret, and E. Deleporte. Strong exciton-photon coupling in a microcavity containing layered perovskite semiconductors. *Applied Physics Letters*, 89(17):171110, oct 2006.
- [21] T. Low, A. Chaves, J. D. Caldwell, A. Kumar, N. X. Fang, P. Avouris, T. F. Heinz, F. Guinea, L. Martin-Moreno, and F. Koppens. Polaritons in layered two-dimensional materials. *Nature Materials*, 16(2):182–194, Nov 2016.
- [22] F. Lédée, G. Trippé-Allard, H. Diab, P. Audebert, D. Garrot, J.S. Lauret, and E. Deleporte. Fast growth of monocrystalline thin films of 2d layered hybrid perovskite. *CrystEngComm*, 19(19):2598–2602, 2017.
- [23] M. Wouters and I. Carusotto. Excitations in a nonequilibrium bose-einstein condensate of exciton polaritons. *Phys. Rev. Lett.*, 99:140402, Oct 2007.
- [24] C. Ciuti, P. Schwendimann, B. Deveaud, and A. Quattropani. Theory of the angle-resonant polariton amplifier. *Phys. Rev. B*, 62:R4825–R4828, Aug 2000.
- [25] M. Vladimirova, S. Cronenberger, D. Scalbert, K. V. Kavokin, A. Miard, A. Lemaître, J. Bloch, D. Solnyshkov, G. Malpuech, and A. V. Kavokin. Polariton-polariton interaction constants in microcavities. *Phys. Rev. B*, 82:075301, Aug 2010.
- [26] M. Vladimirova, S. Cronenberger, D. Scalbert, M. Nawrocki, A. V. Kavokin, A. Miard, A Lemaître, and J. Bloch. Polarization controlled nonlinear transmission of light through semiconductor microcavities. *Phys. Rev. B*, 79:115325, Mar 2009.
- [27] D. Ballarini, A. Amo, and L. Viña. Transition from the strong- to the weak-coupling regime in semiconductor microcavities: Polarization dependence. *Applied Physics Letters*, 2(6):90, 201905, May 2007.
- [28] A. Fieramosca, L. De Marco, M. Passoni, L. Polimeno, A. Rizzo, B. L. T. Rosa, G. Cruciani, L. Dominici, M. De Giorgi, G. Gigli, L. C. Andreani, D. Gerace, D. Ballarini, and D. Sanvitto. Tunable out-of-plane excitons in 2d single-crystal perovskites. *ACS Photonics*, 5:4179–4185, Sep 2018.
- [29] D. Giovanni, W. K. Chong, H. A. Dewi, K. Thirumal, I. Neogi, R. Ramesh, S. Mhaisalkar, N. Mathews, and T. C. Sum. Tunable room-temperature spin-selective optical stark effect in solution-processed layered halide perovskites. *Science Advances*, 2(6):e1600477–e1600477, Jun 2016.

- [30] P. M. Walker, L. Tinkler, D. V. Skryabin, A. Yulin, B. Royall, I. Farrer, D. A. Ritchie, M. S. Skolnick, and D. N. Krizhanovskii. Ultra-low-power hybrid light–matter solitons. *Nature Communications*, 6(1), Sep 2015.
- [31] P. M. Walker, L. Tinkler, B. Royall, D. V. Skryabin, I. Farrer, D. A. Ritchie, M. S. Skolnick, and D. N. Krizhanovskii. Dark solitons in high velocity waveguide polariton fluids. *Phys. Rev. Lett.*, 119:097403, Aug 2017.
- [32] K. S. Daskalakis, S. A. Maier, R. Murray, and S. Kéna-Cohen. Nonlinear interactions in an organic polariton condensate. *Nature Materials*, 13(3):271–278, Feb 2014.